Picosecond and Steady-State Emission of $[Ru(phen)_2dppz]^{2+}$ in Glycerol: Anomalous Temperature Dependence

Björn Önfelt,* Johan Olofsson, Per Lincoln, and Bengt Nordén

Physical Chemistry, Department of Chemistry and Bioscience, Chalmers University of Technology, S-412 96 Gothenburg, Sweden

Received: September 6, 2002; In Final Form: November 20, 2002

The excited-state deactivation of the "light-switch" compound $[Ru(phen)_2dppz]^{2+}$, where phen = 1,10-phenanthroline and dppz = dipyrido[3,2-a:2′,3′-c]phenazine, has been investigated in glycerol using single-photon counting at picosecond time resolution. Relaxation back to the ground state occurs in about 8 ns at 20 °C, which is much faster than previously reported in monohydric alcohols, though still slow compared to that in water. Multivariate kinetic analysis reveals three distinct excited species involved in the relaxation process in glycerol. Using a matrix exponential approach for the kinetic data analysis, including global fitting of the relaxation data collected at many wavelengths, individual emission spectra for all three excited species could be resolved. The resolved emission profile for the most short-lived species was found to resemble the steady-state emission spectrum of $[Ru(phen)_3]^{2+}$ in glycerol whereas the emission profile of the intermediate species resembled that of $[Ru(phen)_2dppz]^{2+}$ in ethanol. The spectrum of the third species is considerably red-shifted compared to those of the other two. The longest lifetime as well as the emission quantum yield show pronounced nonmonotonic variations with temperature in apparent conflict with the Arrhenius equation. This anomalous temperature dependence can be accounted for by a model based on the equilibrium between two excited species, corresponding to the two resolved emission spectra retrieved at 20 °C. Thermodynamic data indicates that transfer to the fast-relaxing, red-shifted species is accompanied by a substantial lowering in enthalpy. The thermodynamic data, as well as an abnormally high preexponential factor for the back reaction from the third to the second excited species, could be explained in terms of the formation of two hydrogen bonds, one to each of the aza nitrogens of the dppz moiety.

Introduction

Transition-metal complexes with nitrogen-containing aromatic ligands have attracted attention because of their ample variation possibilities of forming interesting 3D structures, which are often hard to match with standard organic stereochemistry. In particular, they have been used in the search for complexes with specific binding to DNA.[1,2] Many transition-metal complexes often also exhibit interesting photophysical properties and are rich in states and transitions of varying nature.[3−5] A particular interesting class of compounds that has been extensively studied in recent years is $[Ru(L)_2dppz]^{2+}$,[6,7] where L is either bpy or phen (bpy = 2,2′-bipyridine, phen = 1,10-phenanthroline, and dppz = dipyrido[3,2-a:2′,3′-c]phenazine). Its DNA binding properties have been well characterized,[8−18] and several new compounds containing the $Ru(phen)_2dppz$ chromophore as a building block have been constructed in the search for unique DNA binders.[19−22] A property that has attracted particular attention is the large increase in the quantum yield and excited-state lifetime that is connected with the DNA binding of the compound in water solution and which has been named the "light switch effect".[7,18] A longer lifetime is also observed in organic solvents such as acetonitrile and ethanol[23,24] whereas in water solution the emission is practically completely quenched.[25−28]

The photophysics of the basic polypyridyl Ru(II) chromophore is rather well understood. Upon excitation with visible light, an electron is transferred from a d orbital localized on the ruthenium to an unoccupied π^* orbital on either of the three bidentate ligands so that a metal-to-ligand charge transfer (MLCT) state is formed.[3,29−32] For $[Ru(L)_2dppz]^{2+}$ (where L is either phen or bpy), it has been concluded that the lowest MLCT state is one with the electron localized on the dppz ligand.[6,24,28,33] Investigations of the temperature dependence of the excited-state lifetime of several polypyridyl Ru(II) complexes have shown that relaxation can occur by the thermal population of both metal-centered (MC) and close-lying MLCT states.[4,34−37] The rate of nonradiative decay has also been studied in terms of the energy-gap law for MLCT states.[5,38−41]

Recent time-resolved measurements of $[Ru(phen)_2dppz]^{2+}$ dissolved in water have revealed dynamics on the picosecond timescale, eventually yielding an equilibrated MLCT state of triplet character that experience an ∼260 ps radiationless decay to the ground state.[25−27,42−44] Several studies have demonstrated the existence of at least one intermediate MLCT state that is distinctly different from the lowest excited state.[25−27,42−44] Ultrafast measurements on the parent chromophore $[Ru(bpy)_3]^{2+}$ have shown that intersystem crossing is associated with a time constant of less than 100 fs,[45,46] so the intersystem crossing in $[Ru(phen)_2dppz]^{2+}$ is concluded to be faster than any process observed for this chromophore.[25−27,42−44] The intermediate MLCT state in water has been suggested to be similar to that dominating the emission in acetonitrile and DNA,[25] a proposal supported by time-resolved resonance Raman studies.[26,44] Rather large differences in the resonance Raman spectra of the lowest

* To whom correspondence should be addressed. E-mail: onfelt@phc.chalmers.se. Tel: +46-31-772-51-20. Fax: +46-31-772-38-58.

10.1021/jp0269266 CCC: $25.00
Published on Web 01/21/2003

excited state have been observed for $[Ru(phen)_2dppz]^{2+}$ in the presence of DNA compared to that for acetonitrile solution,[26,44] possibly reflecting the sensitivity of the electronic structure to interactions with the solvent. The interconversion between states was suggested to be somehow associated with, or possibly even rate-limited by, the reorientation of water molecules engaged in hydrogen bond formation to the aza lone pairs on the reduced dppz ligand.[25,27]

The excited-state dynamics prior to ground-state relaxation has also been observed in methanol,[26,43,47] ethanol,[44,47] and acetonitrile,[26,43] where the compound does not experience rapid relaxation to the ground state, indicating a more complex mechanism than originally proposed,[25] involving a "precursor" state.[26,44]

In this study, we report the finding that a fast and efficient deactivation may also occur in organic solvents such as glycerol, although not nearly as fast as in water. Our results support a mechanism involving three excited states, all of MLCT character. Time-correlated single-photon counting (TCSPC) measurements show that the interconversion between states is significantly slower in glycerol than what has been reported in other solvents,[26,27,43,44] possibly as a consequence of the higher viscosity. The rate of interconversion between the excited states as well as the emission quantum yields show pronounced nonmonotonic variations with temperature in apparent conflict with the Arrhenius equation. The emission quantum yield passes through a minimum at about 40 °C, which is also correlated to a minimum of the longest excited-state lifetime and a maximum red shift of the steady-state spectrum. As the temperature is further raised, the emission quantum yield increases and reaches a maximum at about 120 °C before it starts to decrease again. Moving from 40 °C, either up or down in temperature, in both cases leads to an increasing blue shift of the emission spectrum. We shall argue that the anomalous temperature dependence of the emission quantum yield and lifetimes can be accounted for by a model based on two excited species in equilibrium, which are assigned to the respective two species' emission spectra retrieved at 20 °C. On the basis of spectroscopic and kinetic/thermodynamic data, we suggest a mechanism in which specific solvent−solute interactions are crucial for the population decay. In glycerol, we have found a medium in which the partition between a rather long-lived state and one with more-efficient relaxation pathways is delicately balanced, a balance tuned by the temperature.

Materials and Methods

Time-Correlated Single-Photon Counting (TCSPC). Laser pulses (~20 ps duration) were generated from a tunable (700−1000 nm) Ti:saphire oscillator (Tsunami, Spectra Physics 3960) operating at 880 nm with a frequency of 80 MHz. The pulses were passed through a pulse picker (Spectra Physics 3980) that changed the frequency of the pulse train to 4 MHz. The pulses were frequency doubled to 440 nm and passed through a wavelength selector, excluding residual IR, and finally through a (vertical) polarizer to ensure clean polarization of the light used for excitation. Emission was collected at 90° in the horizontal plane relative to the propagation of the excitation beam through a polarizer set at the magic angle from the vertical polarization of the excitation beam. The detection unit was from Edingburough Instruments (OB-900 L) and contained a cell holder thermostated by a water jacket, a monochromator (~16 nm bandwith), and a water-cooled photomultiplier from Hamamatsu (C4878). The instrumental response function was recorded using a dilute sample of a scattering (latex) solution. The recorded fwhm for the response function was ~140 ps (time limited by the detector).

Singular-Value Decomposition. Singular-value decomposition (SVD) analysis was performed using Matlab software. TCSPC decay traces from several wavelengths were organized in a 14 × 3631 matrix (called **M**), with each row of the matrix corresponding to a decay trace at a fixed wavelength and each column serving as a time-gated spectrum. This matrix of time-gate spectra can be decomposed into a product of three matrices according to eq 1:

$$\mathbf{M} = \mathbf{U} \times \mathbf{S} \times \mathbf{V}^{\mathrm{T}} \tag{1}$$

Here, **U** is a 14 × 14 matrix containing the orthogonal spectral components, **S** is a 14 × 14 diagonal matrix with nonnegative singular values (weights of each component) along the diagonal, and **V** is a 3631 × 14 matrix with the time evolution of each component, the superscript T denoting the transpose of the matrix. The value of the diagonal elements of **S** and the time evolution of each component tell how many components are necessary, in principle, to describe all spectra. In this case, three components were found to be significant whereas the rest contained only noise. The time evolution of these three significant components could further be globally fitted to a sum of three exponentials.

Kinetic Analysis. TCSPC traces were fitted to a sum of exponentials ($I(t) = \sum \alpha_i \exp(-t/\tau_i)$, τ being the lifetime) with a deconvolution approach using either the EIS 900 program from Edingbourough Instruments (only individual traces) or a home-made routine in the framework of the software package Matlab, allowing for a global analysis of several traces.

Mechanistic analysis was undertaken by applying the eigenvalue method for solving coupled differential equations, as described in the Appendix, the eigenvalues being the time constants from a global fitting of TCSPC traces. The pre-exponential factors corresponding to each wavelength were used to resolve individual emission spectra for the three excited species (Appendix). This resolution is significantly facilitated by first solving the eigenvalue problem analytically using the lifetimes (eigenvalues) and the corresponding pre-exponential factors determined from global analysis rather than simultaneously fitting the whole data set.

Rate constants coupled to an elementary process should follow an Arrhenius expression ($k_i = A_i \exp(-E_i/RT)$). The Appendix describes the principles for a further test of the kinetic model, in which the variations of the macroscopic time constants, α values, and steady-state intensity with temperature were fitted simultaneously and the microscopic time constants were forced to follow an Arrhenius dependence.

Chemicals. $[Ru(phen)_2dppz]Cl_2$ was synthesized as described elsewhere.[8] Glycerol (99.5%, spectrophotometric grade, water content less than 0.1%) was purchased from Sigma. Degassing of the solution did not change the emission intensity for either $[Ru(phen)_3]^{2+}$ or $[Ru(phen)_2dppz]^{2+}$ in the temperature range of 10−150 °C (see Supporting Information)

Results

Figure 1A shows the time-correlated single-photon-counting decay curves for a series of emission wavelengths, after excitation at 440 nm of $[Ru(phen)_2dppz]^{2+}$ in glycerol at 20 °C, and Figure 1B presents this data as a topological graph. Interestingly, the relaxation to the ground state is quite fast in glycerol compared to that in the lower alcohols[24] and in other polar organic solvents such as acetonitrile[26,43,44] and is ac-

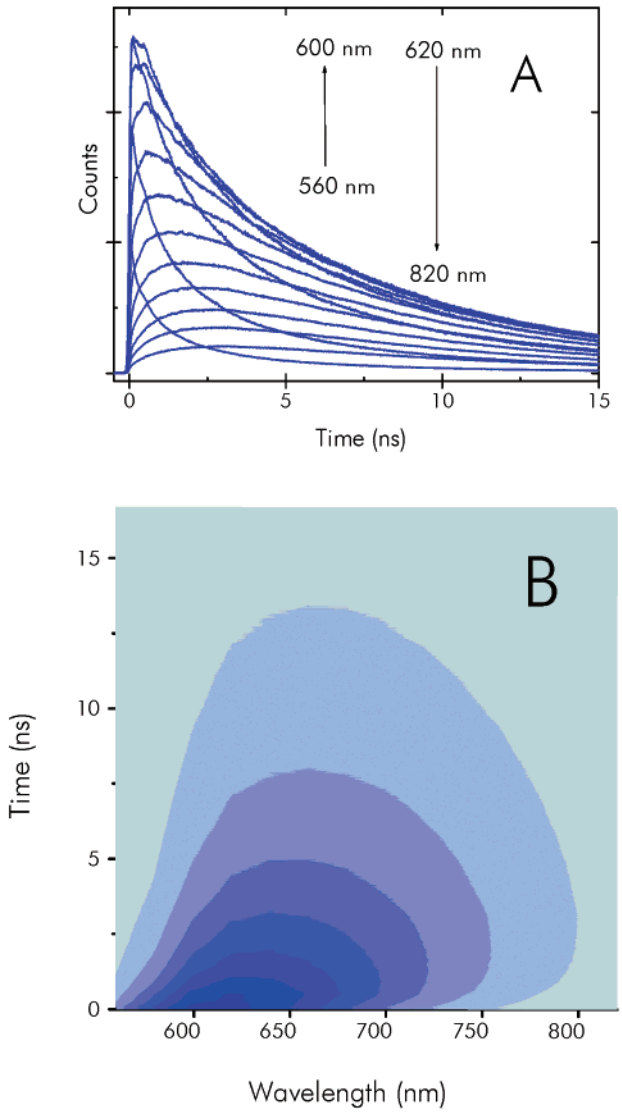

Figure 1. (A) Time-correlated single-photon-counting decay traces of $[Ru(phen)_2dppz]^{2+}$ in glycerol recorded at every 20 nm between 560 and 820 nm. Traces 620−820 nm show a rise followed by a decay. The number of channels was 4048, and the number of counts in the top channel was >30 000 for all traces. (B) Topological graph of the decay as a function of time and wavelength showing the initial red shift.

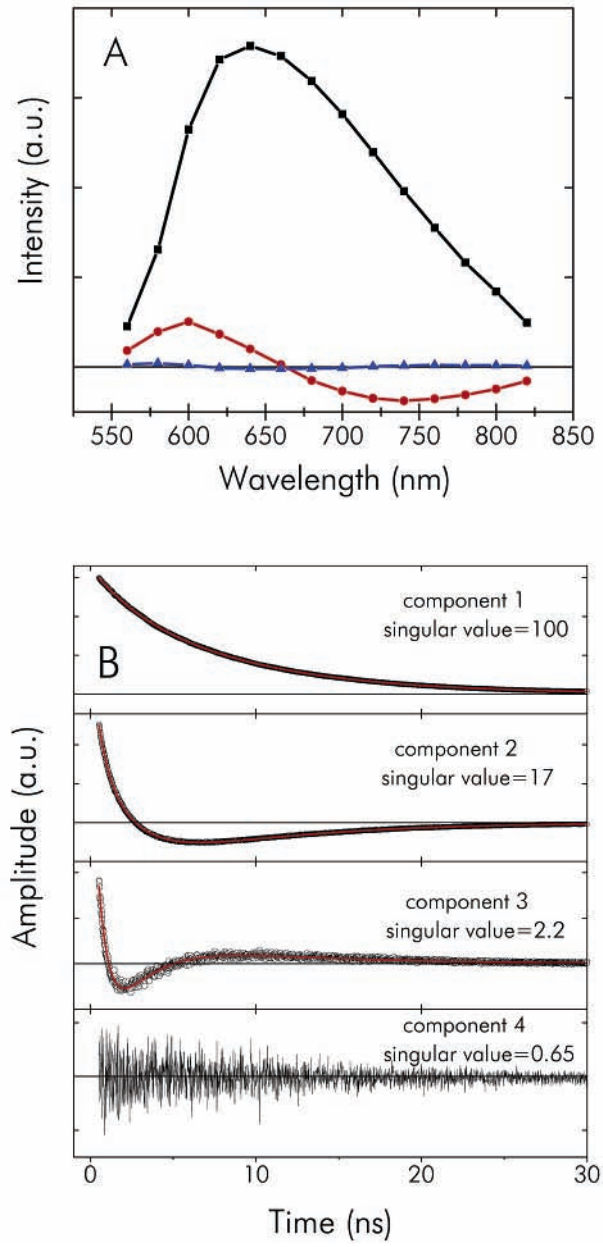

Figure 2. Principal components from SVD analysis. (A) **U** vectors. The three principal components multiplied by their respective singular values. Linear combinations of these may describe all of the time-gated spectra (t > 0.5 ns). (B) **V** vectors. Time evolution of principal components. The fourth component behaves as random noise, confirming that three excited states are sufficient to describe the decay (t > 0.5 ns).

companied by a substantial red shift. Adding a few percent of water to the glycerol solution of $[Ru(phen)_2dppz]^{2+}$ had no significant effect on the steady-state emission intensity, so the contribution from trace amounts of water in the glycerol can be ruled out as a cause of fast relaxation.

Figure 2 shows the result of a singular-value decomposition analysis (SVD, see Methods) of the traces in Figure 1. To eliminate any influence from the shape of the laser pulse, the first 500 ps were removed from the SVD analysis in the first analysis. Three singular-value vectors were found to be markedly more important than the remainder, suggesting that the deactivation process involves three excited species. The plot of the columns of matrix **V** (eq 1) corresponding to the four largest singular values indeed supports this conclusion: it clearly shows that only three of the columns vary with time in a systematic way (Figure 2). Furthermore, an excellent global fit to these three columns could be achieved with a fitting function consisting of a sum of three exponentials, yielding the three lifetimes 0.67, 2.3, and 8.0 ns. Since the data did not include the first 500 ps, the shortest lifetime from this analysis was expected to be less accurate. As an attempt to compensate for this problem, a global fit with a deconvolution of the laser pulse shape was performed both for the full traces recorded at 600, 660, and 740 nm and for the three most significant columns of **V** from an SVD analysis of the full data set. The two fits gave essentially identical sets of three lifetimes: 0.30, 1.85, and 8.06 ns. The whole data set (traces at 14 different wavelengths) could be nicely fitted using these lifetimes, thus providing the pre-exponential factors (α) that were used in the analysis below.

Figure 3A shows the change in the integrated emission intensity for $[Ru(phen)_2dppz]^{2+}$ in glycerol as a function of temperature. Figure 3B shows the quotient between emission intensities at 700 and 600 nm, representing the change in red shift of the emission spectrum, as a function of temperature.

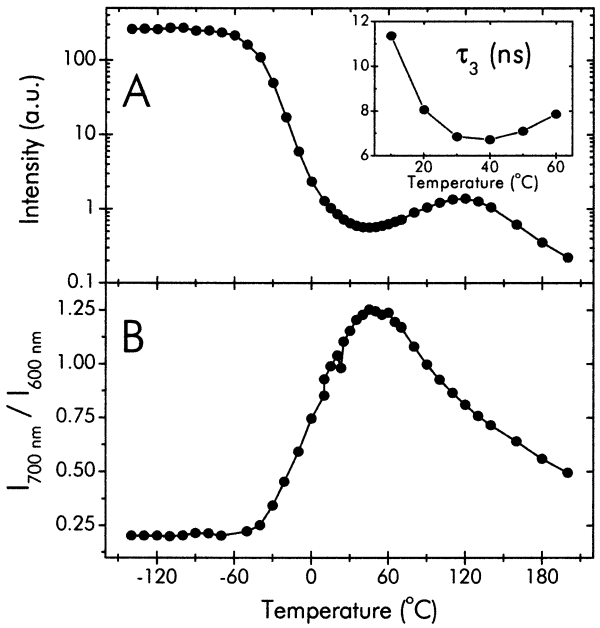

Figure 3. (A) Integrated emission intensity (500−800 nm) as a function of temperature. Up to room temperature, the emission decreases with temperature. By contrast, at 40 °C, the emission intensity increases again, and this change is accompanied by an increase in the longest lifetime. The intensity reaches a maximum at 120 °C before it finally decreases. (B) Ratio between emission intensities at 700 and 600 nm. The maximum at 40 °C, coinciding with the minimum in emission intensity observed in panel A, implies a substantial red shift of the emission maximum. As the temperature is raised above 40 °C, the emission is gradually blue shifted.

TABLE 1: TCSPC Lifetimes of $[Ru(phen)_2dppz]^{2+}$ in Glycerol[a]

temperature (°C)	τ_1 (ns)	τ_2 (ns)	τ_3 (ns)
−20[b]	5.14	33.2	122
10[b]	0.42	2.88	11.35
20	0.30	1.85	8.06
30	0.19	1.24	6.85
40	0.21	0.88	6.72
50	0.12	0.66	7.10
60	0.07	0.37	7.86

[a] Kinetic constants were determined from the global fitting of traces at 600, 660, and 740 nm, except for those at 20 °C where more wavelengths were used in the global fit (see text). [b] Data not included in the analysis because of glass formation of the solvent.

The integrated intensity passes through a minimum at about 40 °C and a maximum around 120 °C. Correspondingly, the quotient I_{700nm}/I_{600nm} has a maximum at 40 °C due to a maximum of the red shift of the emission spectrum at this temperature.

To gain insight into what processes may be the origin of this anomalous temperature dependence, emission decays were measured as a function of temperature in the interval −20 to 60 °C. Table 1 lists the lifetimes found. The two shortest lifetimes could be nicely fitted to an Arrhenius expression for the decay rates ($k = A \exp(-E_a/RT)$, Supporting Information) whereas the longest lifetime varies nonmonotonically, displaying a minimum correlated to a minimum of the emission quantum yield (see inset in Figure 3A).

A nonmonotonic temperature dependence of a single exponential decay to the ground state has previously been reported,[35,48] and for ruthenium complexes with the dipyrido[3,2-c:2′,3′-e]pyridazine (taphen) ligand, the origin of the observation was suggested to be due to two close-lying MLCT states with different charge distributions on the ligand.[35]

SCHEME 1: $[Ru(phen)_2dppz)]^{2+}$

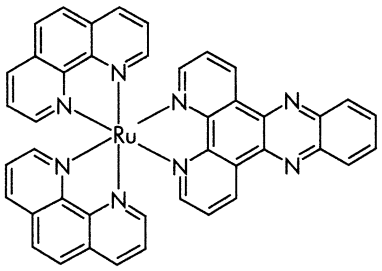

SCHEME 2: Kinetic Model Scheme

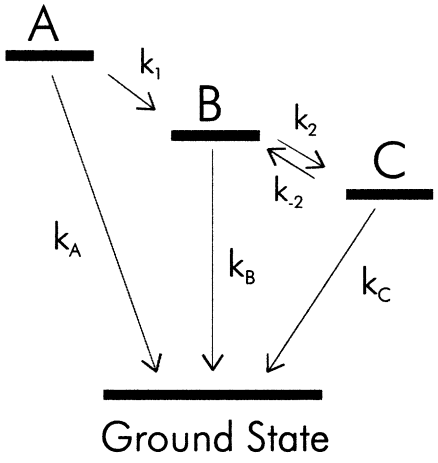

Deactivation Model. The existence of three lifetimes and three SVD components is strong evidence for three distinct excited species involved in the relaxation. Excited-state relaxation mechanisms generally consist of coupled first-order reactions, which means that the observed kinetics may be described as a sum of exponentials. However, the inverses of the observed lifetimes from a fit to a sum of exponentials correspond to true microscopic rate constants only when the mechanism is simple, such as for uncoupled parallel reactions or consecutive and irreversible reactions. Because we have access to relaxation kinetics as well as steady-state spectra at different temperatures, we should be in a position to judge whether a consecutive mechanism could completely account for the observations. As we shall see, the complicated dependence on temperature may be explained by a deactivation mechanism according to Scheme 2, where back-transfer from state C to B is allowed.

Kinetic Modeling. Using a matrix-exponential approach for the kinetic data analysis, described in the Appendix, it was possible to resolve the emission spectra for the three different excited species on the basis of the assumption that the lifetimes that are obtained correspond to the population decay of three excited species: A, B, and C. Since the model involves six parameters and we have access to only three eigenvalues, some rate constants in the mechanism have to be assessed by inference. Thus, the lifetimes in the fit were set equal to that of $[Ru(phen)_3]^{2+}$ in glycerol, thereby assumed to represent the ground-state recovery from state A ($k_A \approx 0.001$ ns^{-1}), and that of $[Ru(phen)_2dppz]^{2+}$ in ethanol, representing the ground-state recovery from B ($k_B \approx 0.01$ ns^{-1}).[23,49] The analysis is found to be relatively insensitive to the choices of k_A and k_B as long as these rates are much smaller than the conversion rate between the states and the total rate of relaxation. By contrast, the size of the rate constant k_C, as expected, strongly affects the values of k_2 and k_{-2}. The rate of recovery from C was estimated from

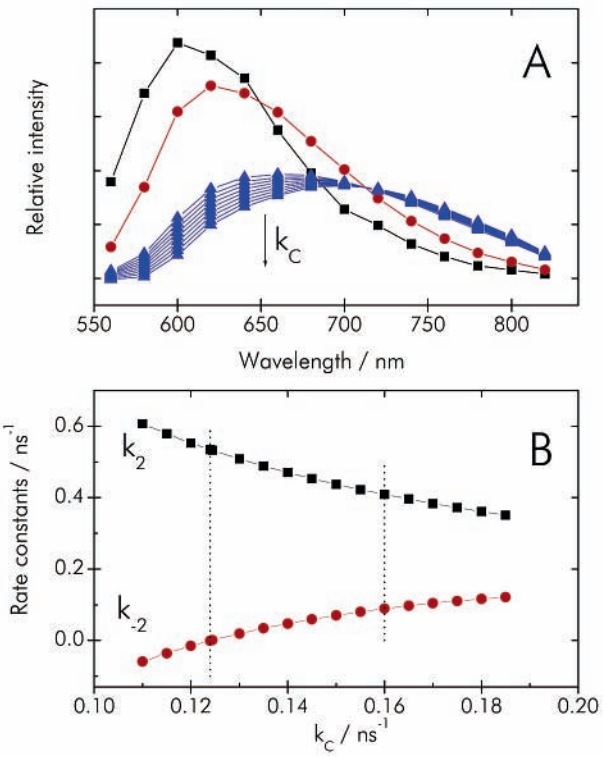

Figure 4. (A) Resolved emission spectra for species A (■), B (●), and C (▲) for varying values of k_C in the interval 0.12−0.16 ns^{-1} (an increasing value of k_C gives a decreased intensity of component C). (B) Calculated rate constants for interconversion between species B and C in Scheme 2 as a function of the choice of k_C. Each set of values is an analytical solution of the eigenvalue problem, where the eigenvalues are the macroscopic lifetimes determined with global analysis ($\tau_1 = 0.30$ ns, $\tau_2 = 1.85$ ns, $\tau_3 = 8.06$ ns). Dotted lines indicate the limits of the interval considered in panel A. Rate constants k_A and k_B were set to 0.001 ns^{-1} and 0.01 ns^{-1}, respectively.

the longest lifetime observed. The range of possible values that k_C may adopt is narrowed further by the prerequisite that $k_{-2} > 0$ and that the spectral components, of course, have to be ≥ 0 at all wavelengths. With those constraints, k_C must be between 0.12 and 0.16 ns^{-1}. Figure 4A shows the emission spectrum components calculated using $k_A = 0.001$ ns^{-1}, $k_B = 0.01$ ns^{-1},[49] and $k_C = 0.12-0.16$ ns^{-1}. Figure 4B shows the calculated values of k_2 and k_{-2} as a function of k_C, using these values for k_A and k_B. Here, each set of values is an analytical solution of the eigenvalue problem, with the eigenvalues being the macroscopic lifetimes obtained from a global analysis ($\tau_1 = 0.30$ ns, $\tau_2 = 1.85$ ns, $\tau_3 = 8.06$ ns). Evidently, at 20 °C, the equilibrium is shifted toward state C, so deactivation takes place dominantly from this species. However, as the temperature is raised, the back reaction from species C to B becomes gradually more important, and B and C are in fast equilibrium, with an equilibrium constant k_2/k_{-2} that rapidly decreases with increasing temperature, leading to the predominance of species B that in turn leads to an increased lifetime and emission intensity as well as a blue shift of the spectrum.

Effects of Temperature. As is seen in Figures 3 and 5, both the emission quantum yield and the measured lifetimes vary with temperature in a nonmonotonic manner. Our objective is a deactivation model that can account for both kinetic and steady-state data. Assuming that the deactivation mechanism is the same and that the emission of the individual states (A, B, and C) is independent of temperature, it should in principle be possible to reconstruct the integrated steady-state emission variation with temperature. Also, the microscopic rate constants

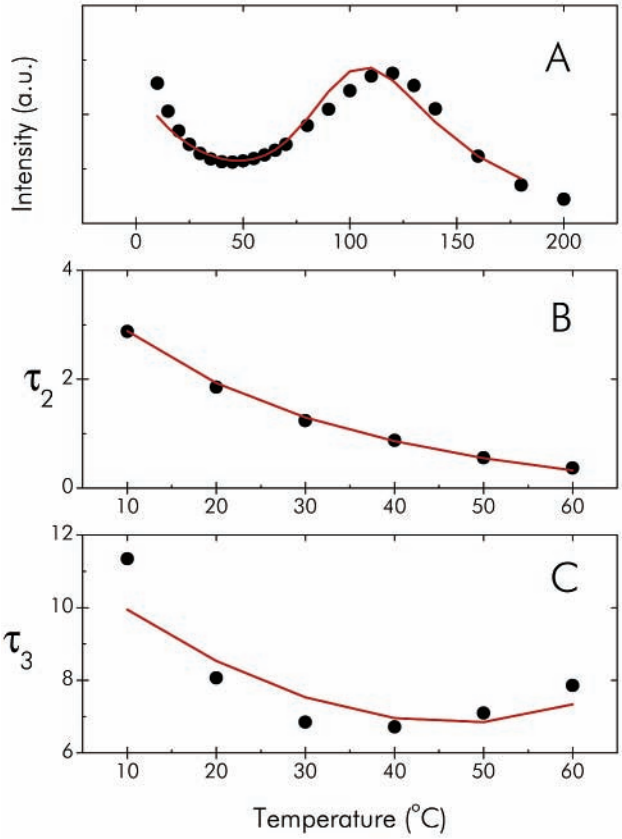

Figure 5. Fit of the temperature data. A mechanism consistent with Scheme 2 fitted to the integrated emission intensity (A), τ_2 (B), and τ_3 (C) as a function of temperature. Microscopic rate constants were forced to follow an Arrhenius dependence.

TABLE 2: Activation Parameters for Microscopic Rate Constants of the Excited-State Relaxation of $[Ru(phen)_2dppz]^{2+}$ in Glycerol according to Scheme 2[a]

process	ln(A/s)	E_a (kJ/mol)
k_2	31 ± 3	27 ± 8
k_{-2}	49 ± 6	79 ± 17
k_B	31 ± 4	46 ± 17
k_C	23 ± 1	9 ± 3

[a] Activation parameters were determined from the fitting of total intensities and macroscopic rate constants as shown in Figure 5.

should be consistent with the macroscopic ones observed, and finally, all rate constants should obey an Arrhenius temperature dependence. We applied a relaxation model according to Scheme 2, including the restrictions as outlined above (see the Appendix). Since the emission of component A has a negligible contribution to the steady-state spectra, the model was simplified to include only the component spectra of B and C. The reasonable fit to the experimental data shows that it is possible to find combinations of rate constants that follow the Arrhenius law and may account for the variation in the steady-state intensity as a function of temperature (see Figure 5, activation parameters listed in Table 2).

If calculated from the Arrhenius parameters, k_C is approximately 0.16 ns^{-1} at 20 °C and is thus consistent with the allowed interval in Figure 4. The size of the activation parameters for k_B, k_C, and k_2 are similar to those reported for other ruthenium complexes.[4,34,37,50] The activation energy for the excited-state decay of $[Ru(phen)_3]^{2+}$ in glycerol, determined from steady-state emission data, is 41 ± 3 kJ/mol (Supporting Information) and is thus in good agreement with that found for k_B (46 ± 17 kJ/mol). However, the activation energy for k_{-2} is

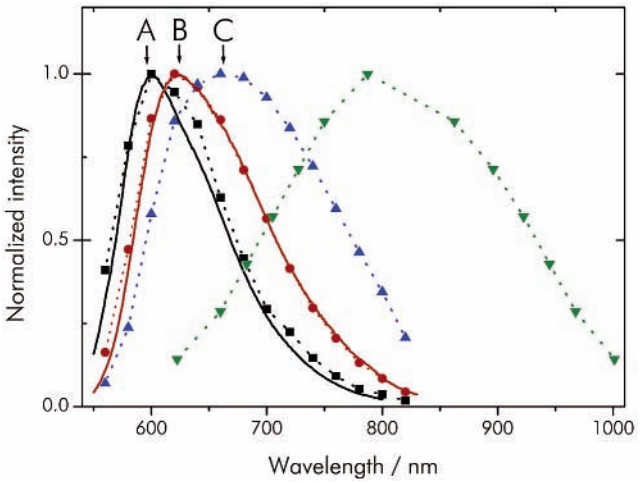

Figure 6. Comparison of spectral profiles. Normalized resolved emission spectra of the three excited species: A (••■••), B (••●••), and C (••▲••). Experimental steady-state emission spectra of $[Ru(phen)_3]^{2+}$ in glycerol, 20 °C (solid black line) and of $[Ru(phen)_2dppz]^{2+}$ in ethanol, 20 °C (solid red line). Note the almost coinciding profiles for the dashed- and solid-line curves. Also shown is a time-gated spectrum (centered at 200 ps from excitation with a time window of about 200 ps) of $[Ru(phen)_2dppz]^{2+}$ in water, reproduced from Olson et al.[25] (••▼••).

high and is accompanied by an extremely high preexponential factor, the origin of which we will return to in the Discussion.

Discussion

In this study, we find, by applying singular-value decomposition to the kinetic analysis of the emission decay trajectories, that the unusually fast excited-state relaxation (beyond 20 ps) of the $[Ru(phen)_2dppz]^{2+}$−glycerol system involves three excited species. Studies of the kinetics, steady-state emission intensity, and energy shift of the emission as a function of temperature suggest that the two lowest excited species are in equilibrium at higher temperatures, consistent with the simple model in Scheme 2. The analysis also allowed the calculation of emission spectra for all the three excited species involved in the relaxation process. The emission components found at 20 °C were combined to fit the variations in emission quantum yield and in the macroscopic kinetic constants with temperature to produce microscopic kinetic constants obeying an Arrhenius dependence. The microscopic rate constants in turn determine the thermodynamic equilibrium constant between species B and C (see below). The activation energies obtained finally allow conclusions to be drawn about the energy differences between the states involved in the relaxation mechanism. On the basis of these thermodynamic, spectral, and activation energy results, we shall argue that the interconversion between species B and C involves specific solvent−solute interactions.

Comparison with $[Ru(phen)_3]^{2+}$ in Glycerol and $[Ru(phen)_2dppz]^{2+}$ in Other Solvents. Figure 6 compares the resolved normalized emission spectra for species A−C (assuming $k_{-2} = 0$) with the steady-state emission spectra of $[Ru(phen)_3]^{2+}$ in glycerol and $[Ru(phen)_2dppz]^{2+}$ in ethanol. Also included in Figure 6 is a time-gated spectrum of $[Ru(phen)_2dppz]^{2+}$ in water reported by Olson et al.[25] It was measured with TCSPC and refers to 200 ps after photoexcitation with a time window of about 200 ps[25] and is thus expected exclusively to reflect the emission spectrum corresponding to the lowest excited state. The similarity between our determined emission spectrum for species A and the steady-state emission spectrum of $[Ru(phen)_3]^{2+}$ in glycerol and between the determined emission spectrum for species B and the experimental spectrum of $[Ru(phen)_2dppz]^{2+}$ in ethanol is obvious. This correlation makes us conclude that species A and B are equivalent to those dominating the emission of $[Ru(phen)_3]^{2+}$ in glycerol and the emission of $[Ru(phen)_2dppz]^{2+}$ in ethanol, respectively (see below). Species C, however, shows properties that are intermediate between those of water and ethanol regarding the wavelength of the emission maximum and the relaxation rate.

Two Luminescent Species. Murphy and co-workers have reported that the rate of nonradiative decay as well as the emission quantum yield for $[Ru(phen)_2dppz]^{2+}$ correlates well with solvent polarity (as measured by the ET parameter[51]) in contrast to a poor correlation with the wavelength of the emission maximum.[23] In 1991, Chambron and Sauvage reported on the luminescence properties of $[Ru(bpy)_2dppz]^{2+}$ in SDS micellar solutions and in alcohols with linear alkyl chains.[24] In the latter study, it was observed that the wavelength of the emission maximum was approximately the same in methanol, ethanol, and propanol whereas the relative emission intensity was 0.06, 1.00, and 1.63, respectively. When going from butanol to decanol, the emission intensity decreased again, now accompanied by a red shift. It is interesting to consider the results from both studies from the perspective of a two-state model, where the steady-state luminescence comes from two species corresponding to B and C in Scheme 2. Low integrated emission intensity, coupled with efficient nonradiative decay, can be explained by the efficient formation of species C. The energy of species C is solvent-dependent,[25,26,44] and by the "energy gap law,"[5,38−41] the more stabilized C is, the more efficiently it is nonradiatively deactivated. This deactivation through the stabilized (red-shifted) species C may seem to be in conflict with the limited red shift of the steady-state emission spectrum observed in, for example, methanol. However, if the nonradiative decay is efficient enough, almost no emission intensity will be detected from species C, and no shift will be observed. Therefore, the steady-state emission in polar solvents (such as methanol) originates almost exclusively from species B. With longer alkyl chains (ethanol, 1-propanol), the emission intensity increases with a small blue shift of λ_{max}, consistent with an equilibrium shift toward B in these solvents. With even longer alkyl chains, the equilibrium shifts toward species C. However, in these solvents, the energy stabilization of species C is not so great, and hence the nonradiative decay is not so efficient, resulting in a red-shifted steady-state spectrum.

Whereas Barbara and co-workers measured time-gated spectra in water,[25] which we may assume originate almost exclusively from the lowest excited state (C), we determine here the emission profile of the species corresponding to the nonradiative decay in glycerol. Preliminary studies in our laboratory indicate that at room temperature the nonradiative decay in ethanol takes place from the same species that dominates the emission.[52] To a first approximation, the energy gap law predicts that the logarithm of the nonradiative decay rate constant should be proportional to the energy difference between the lowest excited state and the ground state.[38−41] A plot of the logarithm of the rate constant for relaxation back to the ground state measured in water, glycerol, and ethanol versus the emission energy maximum of the lowest excited state gives a straight line, indicating that the origin of the light-switch effect is indeed related to the stabilization by the solvation of the lowest excited state and can be described in terms of the energy gap law (Figure 7).

Arrhenius Parameters. The preexponential factor, A, for the back reaction rate constant, k_{-2}, stands out as very high

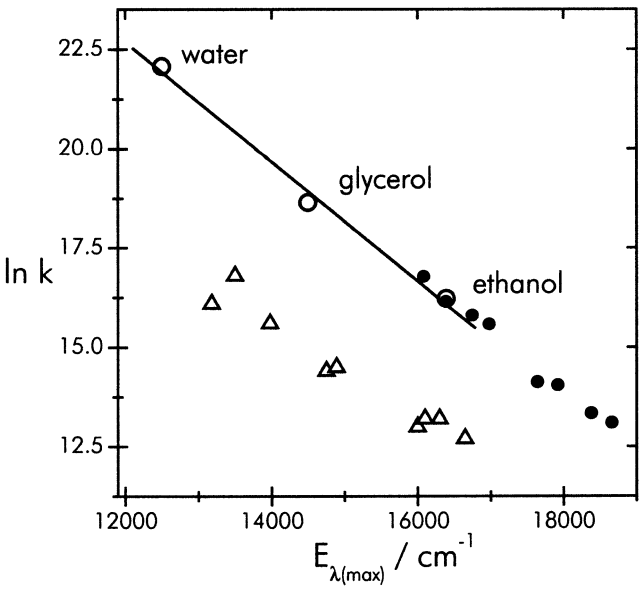

Figure 7. Plot of the natural logarithm of the rate constant for relaxation to the ground state vs the emission maximum corresponding to the lowest excited species for $[Ru(phen)_2dppz]^{2+}$ (○) in ethanol, glycerol, and water (see text). Also plotted are data for $[Ru(bpy)_2L]^{2+}$ for various ligands L (△) reproduced from Barqawi et al.[39] and data for $[Re(bpy)(CO)_3L]$ (●) reproduced from Caspar et al.[40]

compared to the maximum value of the frequency factor of the Eyring theory ($\sim 10^{14}$ s^{-1}). Attempts to force the value to be smaller than the lower error limit gave poor fits. Large values of preexponential factors have been observed in other contexts[53,54] and in our case indicates that the reaction described by k_{-2} is not an elementary reaction. As will be argued below, the explanation for the high preexponential factor is that C → B involves two elementary steps corresponding to the consecutive breaking of a hydrogen bond to each of the two aza-nitrogen lone pairs of the $dppz^{\bullet-}$ anion radical.

The enthalpy difference between species B and C may be obtained from the kinetic data as follows:

$$\ln K = \ln\left(\frac{k_2}{k_{-2}}\right) = \ln\left(\frac{A(k_2)}{A(k_{-2})}\right) + \frac{E_a(k_{-2}) - E_a(k_2)}{RT} \quad (2)$$

$$\Delta G^\circ = \Delta H^\circ - T\Delta S^\circ = -RT \ln K \quad (3)$$

$$\Delta H^\circ = E_a(k_2) - E_a(k_{-2}) = -51 \pm 9 \text{ kJ/mol} \quad (4)$$

$$\Delta S^\circ = R \ln\left(\frac{A(k_2)}{A(k_{-2})}\right) = -150 \pm 25 \text{ J/K mol} \quad (5)$$

Being derived from kinetic data, the thermodynamic constants reflect the difference between the excited species B and C including differences in solvent interactions. The enthalpy of a hydrogen bond between two hydroxyl groups has been estimated to be ~30 kJ/mol.[55] Thus, the value measured here ($\Delta H \approx -51$ kJ/mol) is of the magnitude expected for two hydrogen bonds, suggesting that the process B → C involves the formation of hydrogen bonds to both aza nitrogens of the $dppz^{\bullet-}$ anion radical.

The difference in enthalpy between B and C should not be confused with the spectroscopic energy difference between the emission energies of B and C (an estimate of the energy difference based on the 0−0 transitions at the blue end of the emission spectra gave ~8 kJ/mol, obtained from $\lambda_{00}(B) = 540$ nm and $\lambda_{00}(C) = 560$ nm). The latter energy difference refers to vertical transitions with the preserved solvent geometries of the respective excited states B and C.

SCHEME 3: Schematic Model of Relaxation Pathways[a]

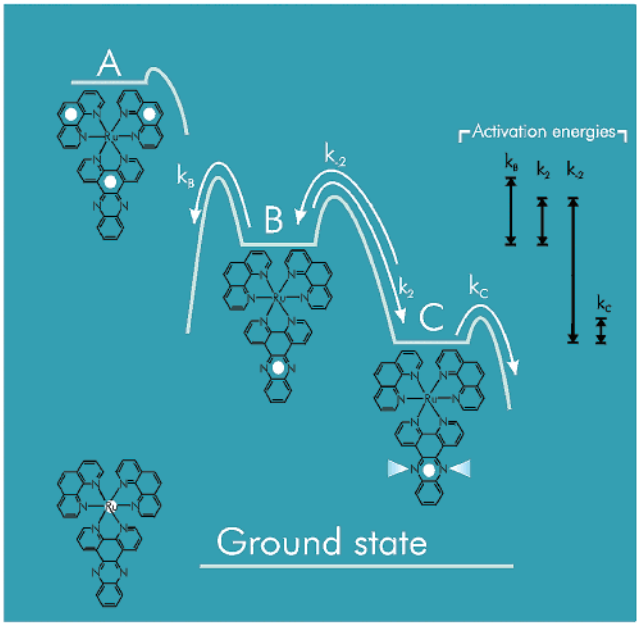

[a] Upon excitation with visible light, a mixture of charge-separated states is formed, and the electron (white ball) is localized in a π^* orbital on either one of the phen ligands or the phen part of the dppz ligand (state A). State A converts to another MLCT state where the electron is localized solely on the dppz ligand (state B). State C involves an organization of solvent including hydrogen bonds to both phenazine nitrogens (triangles). State C is associated with low entropy so that the equilibrium shifts back to state B at higher temperature.

Model—Solvation and Stabilization. The similarity between the emission spectrum of $[Ru(phen)_3]^{2+}$ in glycerol and that of species A makes us postulate that the first species observed (see Scheme 3) may represent a mixture of triplet MLCT states, with the transferred electron being localized on either of the phen ligands or on the phen part of the dppz ligand. This mixture of states quickly ($\tau = 0.3$ ns) converts into another MLCT state (B in Scheme 3), which is similar or identical to the state that dominates the emission in other organic solvents and DNA. This state is characterized by a localization of the electron to a π^* orbital on the dppz ligand.[6,28,33] Thus, the A → B conversion is partly an interligand electron transfer (ILET) process.[56−60] Previous studies of $[Ru(bpy)_3]^{2+}$ report an ILET process of 30 ps in glycerol[60] and 230 ps in ethylene glycol,[57] which should be compared to our value of 300 ps for the A → B conversion. State B is converted into state C, which from kinetic data is found to be associated with a lower enthalpy ($\Delta H^\circ \approx -51$ kJ/mol) as well as entropy ($\Delta S^\circ \approx -150$ J/mol K), explaining why at higher temperature the back reaction dominates.

A three-state model is in qualitative agreement with what we earlier observed for the excited-state decay of $[Ru(phen)_2dppz]^{2+}$ and two other structurally similar complexes in water solution,[27,44] despite a 3 orders of magnitude difference in time constants. The A → B transfer rate was found to be 0.7 ps in water[27] but to be slowed to about 0.3 ns in the present case, possibly caused by the higher viscosity of glycerol (about a factor of 1000 compared to that of water at room temperature). The second phase (B → C) was suggested to be due to the formation of hydrogen bonds of solvent molecules to the phenazine aza nitrogens, which may serve as good hydrogen bond acceptors in the excited state,[25] in which the dppz moiety has the character of an anion radical.[6,24,28,33] In water, the rate

SCHEME 4

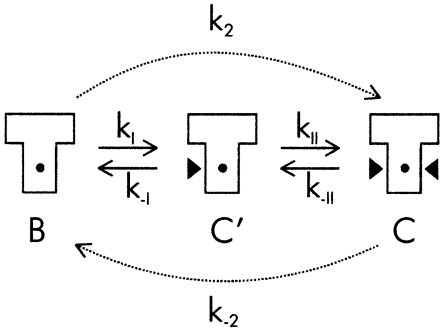

of this process was measured to have an associated time constant of 3−5 ps[25−27,43,44] whereas the corresponding lifetime in glycerol is $(k_2)^{-1} \approx 1.9$ ns. Interestingly, the lifetimes in water coincide with those measured for the slower (diffusive) part of the solvation dynamics measured in water (0.7−1 ps)[61,62] and the biphasic orientational relaxation of water molecules (0.7 and 4 ps).[63,64]

Our conclusion that the interconversion of B → C in glycerol is due to the formation of hydrogen bonds to the aza lone pairs of $dppz^{\bullet-}$ is in line with previous findings in water.[25,27] However, until now, it has not been known whether both aza nitrogens are hydrogen bonded in the stabilized species. Although nonspecific solvation processes are generally found to be faster,[65,66] hydrogen bond formation and breaking in ethylene glycol and glycerol have been reported to be even some 10 times faster than the 1.9 ns we observe here.[67] However, since dppz may be assumed not to form hydrogen bonds in the ground-state complex and the molecules in the first solvation shell are known to rearrange more slowly than the solvent in outer shells[66,68,69] (especially in hydrogen-bonding solvents),[70] hydrogen bond formation is excepted to be slower in the present case.

Also, the exceptionally high preexponential factor of the reverse process C → B ($A(k_{-2}) = 2.4 \times 10^{21}$ s^{-1} in Table 2) may be explained by our hydrogen-bonding model. Let us assume that the process B ⇄ C involves two consecutive hydrogen bond steps, one to each aza nitrogen lone pair (Scheme 4).

In this Scheme, C′ corresponds to the mono-hydrogen-bonded species. If the rate constant k_{II} is only a few times larger than k_I, then the overall process B → C will appear effectively as a single step in our kinetic analysis. In such a case, k_I reflects a rate-limiting step, and the measured rate constant, k_2, is approximately equal to k_I. The equilibrium constant for the reaction between B and C can be expressed as the ratio of the rate constants for the forward and back reactions (eq 6).

$$\frac{k_2}{k_{-2}} = \frac{k_I}{k_{-I}}\frac{k_{II}}{k_{-II}} = \left(\frac{k_I}{k_{-I}}\right)^2 \qquad (6)$$

The last sign of equality holds if we may assume that the two hydrogen bonds have the same stability. Using the fact that $k_I \approx k_2$, a rearrangement of eq 6 gives

$$(k_{-I})^2 = \frac{k_{-2}(k_I)^2}{k_2} = k_{-2}k_2 \Rightarrow k_{-I} = (k_2k_{-2})^{1/2} \qquad (7)$$

and thus for the Arrhenius preexponential factors

$$A(k_{-I}) = (A(k_2)A(k_{-2}))^{1/2} \qquad (8)$$

Insertion of the Arrhenius data (Table 2) into eq 8 gives a preexponential factor of $A(k_{-I}) = 10^{17}$ for the elementary step of a hydrogen bond breakage.

An interesting observation, finally, is the similarity between $[Ru(phen)_3]^{2+}$ and species B of $[Ru(phen)_2dppz]^{2+}$ regarding the activation energy for decay to the ground state. This agreement gives additional support to our hypothesis that species B is not hydrogen-bonded to solvent. In conclusion, the excited-states species A and B of $[Ru(phen)_2dppz]^{2+}$ show similarities to $[Ru(phen)_3]^{2+}$ whereas species C is unique to $[Ru(phen)_2dppz]^{2+}$ in hydrogen-bonding solvents.

Conclusions

We have learned the following from the present study:

(1) Light-switch compound $[Ru(phen)_2dppz]^{2+}$ exhibits a surprisingly efficient quenching in glycerol. Although the ground-state recovery is speeded up in glycerol, compared to that in methanol and ethanol, the interconversion between MLCT states is significantly slowed, allowing for the discrimination of excited intermediates. With the present time resolution, we observe three MLCT excited states, A, B, and C, from which we can resolve individual emission spectra. The resolved emission profiles for the two most short-lived species could be identified with the steady-state spectra of $[Ru(phen)_3]^{2+}$ in glycerol and $[Ru(phen)_2dppz]^{2+}$ in ethanol.

(2) Nonmonotonic variations with temperature for the longest lifetime (τ_3) and the emission quantum yield indicate that the two lowest states, B and C, are in equilibrium with each other at higher temperature.

(3) The previously observed[23,24] poor correlation between the nonradiative rate and emission energy maximum in various solvents can be explained by the coexistence of two emissive states with different emission maxima and nonradiative decay rates. The resolution of the emission spectrum corresponding to the lowest excited state results in relaxation behavior that is consistent with the energy gap law.

(4) Kinetic data indicate that transfer to the lowest-lying MLCT state is accompanied by a large decrease in enthalpy (corresponding to the establishment of two hydrogen bonds) as well as a significant entropy decrease. Spectroscopic data do not reflect such a large enthalpy change, indicating that a substantial energy contribution comes from solvent interactions. More specifically, the results support a model in which the final excited state, C, is stabilized by hydrogen bonds from solvent OH hydrogens to both of the two aza nitrogens of the $dppz^{\bullet-}$ anion radical moiety.

Acknowledgment. This cost of this study was defrayed by a grant to B.N. from the Swedish Science Research Council (VR).

Appendix

Eigenvalue Method for the Analysis of Kinetic Data. Excited-state relaxation processes involve in most cases a system of first-order reactions. If several excited states are involved and there are several relaxation pathways, the measured (macroscopic) rate constants can be different from the true (microscopic) rate constants. However, for a suggested mechanism, it is possible to find solutions of the microscopic rate constants that are mathematically consistent with the observed, macroscopic constants. Any kinetic process of several first-order reactions can be described by a sum of exponentials ($I(t) = \sum\alpha_i \exp(-t/\tau_i)$, τ being the lifetime), and the number of exponentials required is directly related to the number of intermediates involved in the mechanism. The rates of the

reactions involved in Scheme 2 can be described with the equations given below:

$$\frac{d[A]}{dt} = -(k_1 + k_A)[A] \tag{A1}$$

$$\frac{d[B]}{dt} = k_1[A] + k_{-2}[C] - (k_2 + k_B)[B] \tag{A2}$$

$$\frac{d[C]}{dt} = k_2[B] - (k_{-2} + k_C)[C] \tag{A3}$$

$$\frac{d[GS]}{dt} = k_A[A] + k_B[B] + k_C[C] \tag{A4}$$

These equations can be expressed in matrix notation as follows: We introduce a column vector **q** that contains the concentrations of the different states and a matrix **K** that contains the microscopic rate constants to get eq A.5.

$$\frac{d\mathbf{q}}{dt} = \begin{bmatrix} -(k_A+k_1) & 0 & 0 & 0 \\ k_1 & -(k_B+k_2) & k_{-2} & 0 \\ 0 & k_2 & -(k_C+k_{-2}) & 0 \\ k_A & k_B & k_C & 0 \end{bmatrix} \begin{bmatrix} [A]_t \\ [B]_t \\ [C]_t \\ [GS]_t \end{bmatrix} = \mathbf{Kq} \tag{A5}$$

After integration, we get

$$\mathbf{q}_t = \text{expm}\,(\mathbf{K}t)\mathbf{q}_0 \tag{A6}$$

where

$$\mathbf{q}_0 = \begin{bmatrix} [A]_0 \\ [B]_0 \\ [C]_0 \\ [GS]_0 \end{bmatrix} \tag{A7}$$

and expm denotes taking the matrix exponential of its argument. The measured (macroscopic) rate constants are the negative eigenvalues of matrix **K**, and since the eigenvalues thus are distinct, **K** can be diagonalized by its eigenvector matrix **W**:

$$\mathbf{W}^{-1}\mathbf{K}\mathbf{W} = \Lambda = \begin{bmatrix} 0 & 0 & 0 & 0 \\ 0 & \lambda_1 & 0 & 0 \\ 0 & 0 & \lambda_2 & 0 \\ 0 & 0 & 0 & \lambda_3 \end{bmatrix} \tag{A8}$$

Then

$$\mathbf{K} = \mathbf{W}\Lambda\mathbf{W}^{-1} \tag{A9}$$

and the matrix exponential of $\mathbf{K}\cdot t$ may be defined as

$$\text{expm}(\mathbf{K}t) = \mathbf{W}\,\exp(\Lambda t)\mathbf{W}^{-1} \tag{A10}$$

where

$$\exp(\Lambda t) = \begin{bmatrix} e^{0t} & 0 & 0 & 0 \\ 0 & e^{\lambda_1 t} & 0 & 0 \\ 0 & 0 & e^{\lambda_2 t} & 0 \\ 0 & 0 & 0 & e^{\lambda_3 t} \end{bmatrix} \tag{A11}$$

Alternatively, $\mathbf{q}_t$ may be expressed as

$$\mathbf{q}_t = \mathbf{W}\,\exp(\Lambda t)\mathbf{W}^{-1}\mathbf{q}_0 = \mathbf{W}\,\text{diag}(\mathbf{W}^{-1}\mathbf{q}_0)\begin{bmatrix} e^{0t} \\ e^{\lambda_1 t} \\ e^{\lambda_2 t} \\ e^{\lambda_3 t} \end{bmatrix} \tag{A12}$$

where diag denotes a diagonal matrix. The observed TCSPC traces at a specific wavelength and time can be expressed as a sum of exponentials:

$$I_{wl,t} = \alpha_0 + \sum_i \alpha_i \exp(\lambda_i t) \tag{A13}$$

The TCSPC signals (I) at several wavelengths, corrected for the detector's wavelength-dependent sensitivity, may be collected into a matrix (**M**) and be analyzed globally to obtain the macroscopic rate constants in a matrix formulation:

$$\mathbf{M}_{wl,t} = [\alpha_{0,wl}\ \ \alpha_{1,wl}\ \ \alpha_{2,wl}\ \ \alpha_{3,wl}]\begin{bmatrix} e^{0t} \\ e^{\lambda_1 t} \\ e^{\lambda_2 t} \\ e^{\lambda_3 t} \end{bmatrix} = \mathbf{PE} \tag{A14}$$

However, **M** can also be factored as the product of matrix **B** with the emission spectra (at unit concentration) of species A, B, C, and GS (the later, of course, being zero) multiplied with the time evolution of the concentrations:

$$\mathbf{M}_{wl,t} = [S_{A,wl}\,S_{B,wl}\,S_{C,wl}\,S_{GS,wl}]\mathbf{q}_t = \mathbf{B}\mathbf{q}_t \tag{A15}$$

where $S_A - S_{GS}$ are the emission spectra for the respective component. We have

$$\mathbf{M} = \mathbf{PE} = \mathbf{B}\mathbf{q}_t = \mathbf{BW}\,\text{diag}(\mathbf{W}^{-1}\mathbf{q}_0)\mathbf{E} \tag{A16}$$

thus

$$\mathbf{P} \equiv \mathbf{BW}\,\text{diag}(\mathbf{W}^{-1}\mathbf{q}_0) \tag{A17}$$

and

$$\mathbf{P}\,\text{diag}(\mathbf{W}^{-1}\mathbf{q}_0)^{-1}\mathbf{W}^{-1} = \mathbf{B} \tag{A18}$$

which allows **B** to be calculated when **K** and hence the eigenvector matrix **W** are known.

Integrating eq A14 gives the steady-state intensity as

$$I_{SS} = -\sum_i \frac{\alpha_i}{\lambda_i} \tag{A19}$$

Inserting eq A17 gives the steady-state intensity in terms of the microscopic rate constants

$$I_{SS} = -\mathbf{B}\cdot\mathbf{L}^{-1}\mathbf{q}_0 \tag{A20}$$

where **L** is the submatrix formed from **K** by deleting the last row and column.

Temperature Dependence. Since the contribution of state A to the steady-state emission was negligibly small, only the rate constants from species B and C were included in the modeling of the temperature dependence. Assuming each of the four rate constants k_B, k_C, k_2, and k_{-2} to follow the Arrhenius equation

$$k_i = A_i \exp(-E_i/RT) \tag{A21}$$

the temperature dependence of lifetimes $1/\lambda_2$ and $1/\lambda_3$ could be obtained from the eigenvalues of the 2×2 matrix:

$$\mathbf{L} = \begin{bmatrix} -(k_B + k_2) & k_{-2} \\ k_2 & -(k_C + k_2) \end{bmatrix} \tag{A22}$$

From the eigenvector matrix of **L** and the normalized pre-exponential factors α_2 and α_3 of the analysis of the TCSPC traces, the relative emission intensities in the corresponding row vector **B** could be calculated with eq A18 at the different temperatures. Although the elements of **B** calculated this way were found to show some temperature dependence, they could be required to be nonnegative. Last, the dependence of the steady-state intensity (the integrated emission spectra) on temperature was obtained from eq A20:

$$I_{SS} = -[1\ \Phi]\cdot\mathbf{L}^{-1}\begin{bmatrix}1\\0\end{bmatrix} = \frac{k_C + k_{-2} + \Phi k_2}{k_B k_C + k_2 k_C + k_B k_{-2}} \qquad \text{(A23)}$$

where ϕ is the relative integrated emission intensity of species C relative to that of species B.

The four frequency factors A_i and four activation energies E_i were thus varied by applying a nonlinear minimization routine to obtain the best simultaneous fit of the lifetimes in the temperature interval 10−60 °C and steady-state intensities in the interval 10−175 °C, with the additional restraint that **B** calculated from α_2 and α_3 should be nonnegative.

Supporting Information Available: Observed rate constants and pre-exponential factors of the deactivation of $[Ru(phen)_2dppz]^{2+}$ in glycerol as a function of temperature. Integrated emission intensity as a function of temperature for $[Ru(phen)_3]^{2+}$ in glycerol. This material is available free of charge via the Internet at http://pubs.acs.org.

References and Notes

(1) Erkkila, K. E.; Odom, D. T.; Barton, J. K. *Chem. Rev.* **1999**, *99*, 2777−2795.

(2) Nordén, B.; Lincoln, P.; Åkerman, B.; Tuite, E. In *Metal Ions in Biological Systems*; Siegel, A., Siegel, H., Eds.; Marcel Dekker: New York, 1996; Vol. 33, pp 177−252.

(3) Krausz, E.; Ferguson, J. *Prog. Inorg. Chem.* **1989**, *37*, 293−390.

(4) Forster, L. S. *Coord. Chem. Rev.* **2002**, *227*, 59−92.

(5) Chen, P. Y.; Meyer, T. J. *Chem. Rev.* **1998**, *98*, 1439−1477.

(6) Chambron, J.-C.; Sauvage, J.-C.; Amouyal, E.; Koffi, P. *Nouv. J. Chim.* **1985**, *9*, 527−529.

(7) Friedman, A. E.; Chambron, J.-C.; Sauvage, J.-P.; Turro, N. J.; Barton, J. K. *J. Am. Chem. Soc.* **1990**, *112*, 4960−4962.

(8) Hiort, C.; Lincoln, P.; Nordén, B. *J. Am. Chem. Soc.* **1993**, *115*, 3448−3454.

(9) Lincoln, P.; Broo, A.; Nordén, B. *J. Am. Chem. Soc.* **1996**, *118*, 2644−2653.

(10) Haq, I.; Lincoln, P.; Suh, D.; Nordén, B.; Chowdhry, B. Z.; Chaires, J. B. *J. Am. Chem. Soc.* **1995**, *117*, 4788−4796.

(11) Choi, S. D.; Kim, M. S.; Kim, S. K.; Lincoln, P.; Tuite, E.; Nordén, B. *Biochemistry* **1997**, *36*, 214−223.

(12) Holmlin, R. E.; Stemp, E. D. A.; Barton, J. K. *Inorg. Chem.* **1998**, *37*, 29−34.

(13) Tuite, E.; Lincoln, P.; Nordén, B. *J. Am. Chem. Soc.* **1997**, *119*, 239−240.

(14) Dupureur, C. M.; Barton, J. K. *J. Am. Chem. Soc.* **1994**, *116*, 10286−10287.

(15) Dupureur, C. M.; Barton, J. K. *Inorg. Chem.* **1997**, *36*, 33−43.

(16) Hartshorn, R. M.; Barton, J. K. *J. Am. Chem. Soc.* **1992**, *114*, 5919−5925.

(17) Jenkins, Y.; Friedman, A. E.; Turro, N. J.; Barton, J. K. *Biochemistry* **1992**, *31*, 10809−10816.

(18) Friedman, A. E.; Kumar, C. V.; Turro, N. J.; Barton, J. K. *Nucleic Acids Res.* **1991**, *19*, 2595−2602.

(19) Lincoln, P.; Nordén, B. *Chem. Commun.* **1996**, 2145−2146.

(20) Önfelt, B.; Lincoln, P.; Nordén, B. *J. Am. Chem. Soc.* **2001**, *123*, 3630−3637.

(21) Önfelt, B.; Lincoln, P.; Nordén, B. *J. Am. Chem. Soc.* **1999**, *121*, 10846−10847.

(22) Önfelt, B.; Göstring, L.; Lincoln, P.; Nordén, B.; Önfelt, A. *Mutagenesis* **2002**, *17*, 317−320.

(23) Nair, R. B.; Cullum, B. M.; Murphy, C. J. *Inorg. Chem.* **1997**, *36*, 962−965.

(24) Chambron, J. C.; Sauvage, J. P. *Chem. Phys. Lett.* **1991**, *182*, 603−607.

(25) Olson, E. J. C.; Hu, D.; Hörmann, A.; Jonkman, A. M.; Arkin, M. R.; Stemp, E. D. A.; Barton, J. K.; Barbara, P. F. *J. Am. Chem. Soc.* **1997**, *119*, 11458−11467.

(26) Coates, C. G.; Olofsson, J.; Coletti, M.; McGarvey, J. J.; Önfelt, B.; Lincoln, P.; Norden, B.; Tuite, E.; Matousek, P.; Parker, A. W. *J. Phys. Chem. B* **2001**, *105*, 12653−12664.

(27) Önfelt, B.; Lincoln, P.; Nordén, B.; Baskin, J. S.; Zewail, A. H. *Proc. Natl. Acad. Sci. U.S.A.* **2000**, *97*, 5708−5713.

(28) Amouyal, E.; Homsi, A.; Chambron, J.-C.; Sauvage, J.-P. *J. Chem. Soc., Dalton Trans.* **1990**, *6*, 1841−1845.

(29) Kober, E. M.; Sullivan, B. P.; Meyer, T. J. *Inorg. Chem.* **1984**, *23*, 2098−2104.

(30) Kober, E. M.; Meyer, T. J. *Inorg. Chem.* **1982**, *21*, 3967−3977.

(31) Karki, L.; Hupp, J. T. *Inorg. Chem.* **1997**, *36*, 3318−3321.

(32) Bradley, P. G.; Kress, N.; Hornberger, B. A.; Dallinger, R. F.; Woodruff, W. H. *J. Am. Chem. Soc.* **1981**, *103*, 7441−7446.

(33) Schoonover, J. R.; Bates, W. D.; Meyer, T. J. *Inorg. Chem.* **1995**, *34*, 6421−6422.

(34) Sykora, M.; Kincaid, J. R. *Inorg. Chem.* **1995**, *34*, 5852−5856.

(35) Barigelletti, F.; Juris, A.; Balzani, V.; Belser, P.; Vonzelewsky, A. *J. Phys. Chem.* **1986**, *90*, 5190−5193.

(36) Masschelein, A.; Jacquet, L.; Kirschdemesmaeker, A.; Nasielski, J. *Inorg. Chem.* **1990**, *29*, 855−860.

(37) Barigelletti, F.; Juris, A.; Balzani, V.; Belser, P.; Vonzelewsky, A. *Inorg. Chem.* **1983**, *22*, 3335−3339.

(38) Treadway, J. A.; Loeb, B.; Lopez, R.; Anderson, P. A.; Keene, F. R.; Meyer, T. J. *Inorg. Chem.* **1996**, *35*, 2242−2246.

(39) Barqawi, K. R.; Murtaza, Z.; Meyer, T. J. *J. Phys. Chem.* **1991**, *95*, 47−50.

(40) Caspar, J. V.; Meyer, T. J. *J. Phys. Chem.* **1983**, *87*, 952−957.

(41) Caspar, J. V.; Sullivan, B. P.; Kober, E. M.; Meyer, T. J. *Chem. Phys. Lett.* **1982**, *91*, 91−95.

(42) Ujj, L.; Coates, C. G.; Kelly, J. M.; Kruger, P. E.; McGarvey, J. J.; Atkinson, G. H. *J. Phys. Chem. B* **2002**, *106*, 4854−4862.

(43) Coates, C. G.; Callaghan, P.; McGarvey, J. J.; Kelly, J. M.; Jacquet, L.; Kirsch-De Mesmaeker, A. *J. Mol. Struct.* **2001**, *598*, 15−25.

(44) Olofsson, J.; Önfelt, B.; Lincoln, P.; B., N.; Matousek, P.; Parker, A. W.; Tuite, E. *J. Inorg. Biochem.* **2002**, *91*, 286−297.

(45) Bhasikuttan, A. C.; Suzuki, M.; Nakashima, S.; Okada, T. *J. Am. Chem. Soc.* **2002**, *124*, 8398−8405.

(46) Damrauer, N. H.; Cerullo, G.; Yeh, A.; Boussie, T. R.; Shank, C. V.; McCusker, J. K. *Science (Washington, D.C.)* **1997**, *275*, 54−57.

(47) Önfelt, B.; Lincoln, P.; Norden, B.; Baskin, J. S.; Zewail, A. H. Unpublished results.

(48) Barigelletti, F. *J. Chem. Soc., Faraday Trans.* **1987**, *83*, 1567−1576.

(49) Olofsson, J. Electron-Transfer Mediated by DNA, Licentiate Thesis, Chalmers University of Technology, Gothenburg, Sweden, 2001.

(50) Juris, A.; Barigelletti, F.; Balzani, V.; Belser, P.; Vonzelewsky, A. *Inorg. Chem.* **1985**, *24*, 202−206.

(51) Reichardt, C. *Solvent and Solvent Effects in Organic Chemistry*, 2nd ed.; Verlag Chemie: New York, 1988.

(52) Olofsson, J.; Önfelt, B.; Lincoln, P.; Nordén, B. To be submitted for publication.

(53) Rillema, D. P.; Blanton, C. B.; Shaver, R. J.; Jackman, D. C.; Boldaji, M.; Bundy, S.; Worl, L. A.; Meyer, T. J. *Inorg. Chem.* **1992**, *31*, 1600−1606.

(54) Nordholm, S. *Chem. Phys.* **1985**, *98*, 367−379.

(55) Maskil, H. *The Physical Basis of Organic Chemistry*; Oxford University Press: Oxford, U.K., 1985.

(56) Shaw, G. B.; Brown, C. L.; Papanikolas, J. M. *J. Phys. Chem. A* **2002**, *106*, 1483−1495.

(57) Cooley, L. F.; Bergquist, P.; Kelley, D. F. *J. Am. Chem. Soc.* **1990**, *112*, 2612−2617.

(58) Carroll, P. J.; Brus, L. E. *J. Am. Chem. Soc.* **1987**, *109*, 7613−7616.

(59) Carlin, C. M.; Dearmond, M. K. *J. Am. Chem. Soc.* **1985**, *107*, 53−57.

(60) Malone, R. A.; Kelley, D. F. *J. Chem. Phys.* **1991**, *95*, 8970−8976.

(61) Jarzeba, W.; Walker, G. C.; Johnson, A. E.; Kahlow, M. A.; Barbara, P. F. *J. Phys. Chem.* **1988**, *92*, 7039−7041.

(62) Jimenez, R.; Fleming, G. R.; Kumar, P. V.; Maroncelli, M. *Nature (London)* **1994**, *369*, 471−473.

(63) Woutersen, S.; Bakker, H. J. *Nature (London)* **1999**, *402*, 507−509.

(64) Woutersen, S.; Emmerichs, U.; Bakker, H. J. *Science (Washington, D.C.)* **1997**, *278*, 658−660.

(65) Horng, M. L.; Gardecki, J. A.; Papazyan, A.; Maroncelli, M. *J. Phys. Chem.* **1995**, *99*, 17311−17337.

(66) Barbara, P., F.; Jarzeba, W. *Adv. Photochem.* **1990**, *15*, 1−68.

(67) Yu, J. W.; Berg, M. *Chem. Phys. Lett.* **1993**, *208*, 315−320.

(68) Onsager, L. *Can. J. Chem.* **1977**, *55*, 1819.

(69) Rips, I.; Klafter, J.; Jortner, J. *J. Chem. Phys.* **1988**, *88*, 3246−3252.

(70) Sese, G.; Padro, J. A. *J. Chem. Phys.* **1998**, *108*, 6347−6352.